PALEOCEANOGRAPHY, VOL. 28, 619–632, doi:10.1002/palo.20053, 2013

# Northern and southern hemisphere controls on seasonal sea surface temperatures in the Indian Ocean during the last deglaciation

Yiming V. Wang,[1,2] Guillaume Leduc,[1] Marcus Regenberg,[1] Nils Andersen,[2] Thomas Larsen,[2,3] Thomas Blanz,[1] and Ralph R. Schneider[1,2]

Received 17 January 2013; revised 21 June 2013; accepted 5 September 2013; published 11 October 2013.

[1] Different proxies for sea surface temperature (SST) often exhibit divergent trends for deglacial warming in tropical regions, hampering our understanding of the phase relationship between tropical SSTs and continental ice volume at glacial terminations. To reconcile divergent SST trends, we report reconstructions of two commonly used paleothermometers (the foraminifera *G. ruber* Mg/Ca and the alkenone unsaturation index) from a marine sediment core collected in the southwestern tropical Indian Ocean encompassing the last 37,000 years. Our results show that SSTs derived from the alkenone unsaturation index ($U^{K'}_{37}$) are consistently warmer than those derived from Mg/Ca by ~2–3°C except for the Heinrich Event 1. In addition, the initial timing for the deglacial warming of alkenone SST started at ~15.6 ka, which lags behind that of Mg/Ca temperatures by 2.5 kyr. We argue that the discrepancy between the two SST proxies reflects seasonal differences between summer and winter rather than postdepositional processes or sedimentary biases. The $U^{K'}_{37}$ SST record clearly mimics the deglacial SST trend recorded in the North Atlantic region for the earlier part of the termination, indicating that the early deglacial warming trend attributed to local summer temperatures was likely mediated by changes in the Atlantic Meridional Overturning Circulation at the onset of the deglaciation. In contrast, the glacial to interglacial SST pattern recorded by *G. ruber* Mg/Ca probably reflects cold season SSTs. This indicates that the cold season SSTs was likely mediated by climate changes in the southern hemisphere, as it closely tracks the Antarctic timing of deglaciation. Therefore, our study reveals that the tropical southwestern Indian Ocean seasonal SST was closely linked to climate changes occurring in both hemispheres. The austral summer and winter recorded by each proxy is further supported with seasonal SST trends modeled by Atmosphere–ocean General Circulation Models for our core site. Our interpretation that the alkenone and Mg/Ca SSTs are seasonally biased may also explain similar proxy mismatches observed in other tropical regions at the onset of the last termination.

**Citation:** Wang, Y. V., G. Leduc, M. Regenberg, N. Andersen, T. Larsen, T. Blanz, and R. R. Schneider (2013), Northern and southern hemisphere controls on seasonal sea surface temperatures in the Indian Ocean during the last deglaciation, *Paleoceanography*, *28*, 619–632, doi:10.1002/palo.20053.

## 1. Introduction

[2] The sea surface temperature (SST) evolution in the tropics during glacial terminations is essential for understanding the mechanisms behind rapid climate changes in the past [*Shakun et al*., 2012]. However, notable discrepancies of last deglacial SST timing and magnitudes have been observed among multiple SST studies from tropical Oceans [i.e., *Mix* 2006]. Early work documenting the phase relationship between tropical SSTs based on foraminifera Mg/Ca and continental ice volume during glacial terminations suggest that a tropical SST led over ice volume by several millennia [*Lea et al*., 2000; *Saher et al*., 2009]. This led to the hypothesis that tropical SSTs played a pivotal role for climate change during deglaciations through transferring heat and water vapor from the tropics to higher latitudes [*Lea et al*., 2000; *Rodgers et al*., 2003; *Visser et al*., 2003]. More recent SST records based on alkenone unsaturation index ($U^{K'}_{37}$) have challenged this hypothesis, suggesting that the Eastern equatorial Pacific (EEP) SST were rather responding to changes in the Atlantic Meridional Overturning Circulation (AMOC) [*Kiefer and Kienast*, 2005; *Kienast et al*., 2001; *Kienast et al*., 2006]. Similar warming patterns of foraminifera

Additional supporting information may be found in the online version of this article.

[1]Institute of Geosciences, Christian-Albrechts Universität zu Kiel, Kiel, Germany.
[2]Leibniz-Laboratory for Radiometric Dating and Isotope Research, Christian-Albrechts University of Kiel, Kiel, Germany.
[3]Biogeodynamics and Biodiversity Group, Centre for Advanced Studies of Blanes (CEAB), Spanish Research Council (CSIC), Catalonia, Spain.

Corresponding author: Y. V. Wang, Institute of Geosciences, Christian-Albrechts Universität zu Kiel, Ludewig-Meyn-Str. 10–14, 24118 Kiel, Germany. (ywang@leibniz.uni-kiel.de)


0883-8305/13/10.1002/palo.20053

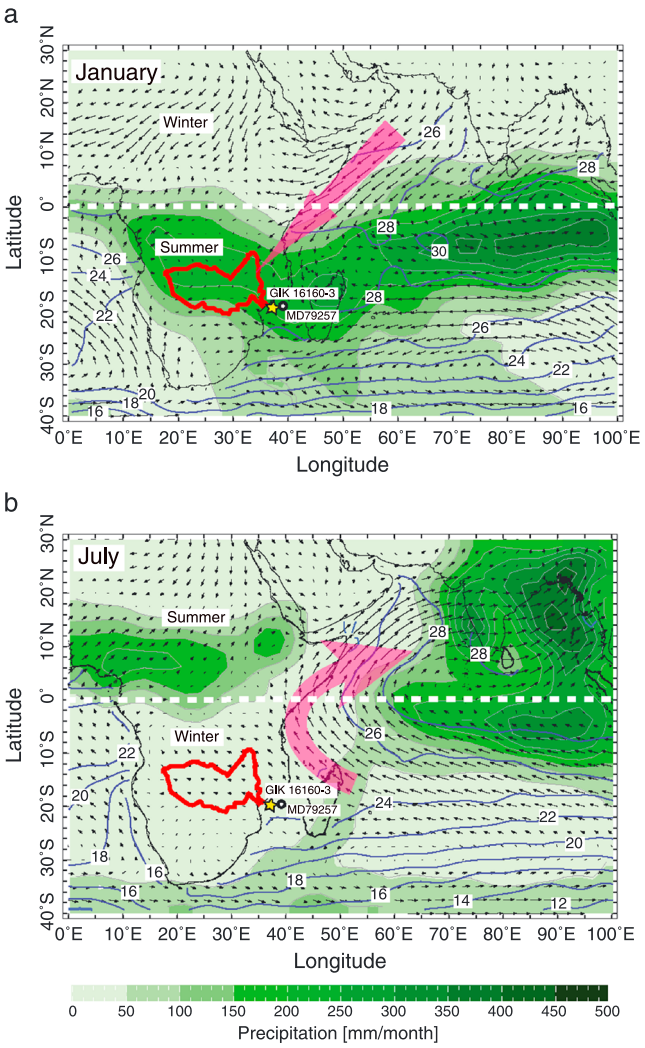


**Figure 1.** Sea surface temperature (SST) field (isotherm in 2°C), amount of precipitation, surface wind direction, and strength over the Indian Ocean and Africa for (a) January and (b) July. The map also shows the position of marine sediment cores GIK16160-3 (yellow star, this study) and MD79275 (white dot) [*Bard et al*., 1997] and the Zambezi river catchment area (red line). The large pink arrows indicate the monsoonal wind directions. Monthly precipitation as well as surface wind speed and strength for the 925 hPa pressure level (arrows with speed proportional to the vectors) is derived from NCEP reanalysis [http://iridl.ldeo.columbia.edu].

Mg/Ca lead $U^{K'}_{37}$ SSTs at terminations in the western equatorial Pacific [*de Garidel-Thoron et al*., 2007; *Kienast et al*., 2001; *Linsley et al*., 2010; *Rosenthal et al*., 2006; *Steinke et al*., 2008; *Visser et al*., 2003]. Although the SST differences are systematic and, in some way, related to identifiable oceanic processes [*Mix*, 2006], it is not yet fully understood what controls such differences between temperature proxies. Several competing hypotheses have been proposed to reconcile mismatches in the Mg/Ca and $U^{K'}_{37}$ SST signals. Those include biases caused by *G. ruber* and alkenone producers' different sensitivities to seasonal or interannual temperature variations, nutrient stress, preservation, postdepositional processes, and artifacts associated with salinity changes [*Koutavas and Sachs*, 2008; *Mix*, 2006; *Saher et al*., 2009]. Recent studies based on paleo data synthesis and model simulations for the Holocene have indicated that tropical $U^{K'}_{37}$ and Mg/Ca-derived SSTs may respond to different seasons [*Leduc et al*., 2010; *Lohmann et al*., 2012; *Schneider et al*., 2010]. However, invoking seasonal preference for reconciling different SST proxies has not been thoroughly tested yet for periods older than the Holocene.

[3] Similar to the Pacific Ocean, the leads and lags of SST evolution in the Indian Ocean during the last deglaciation in relation to the thermal evolution in the high latitudes also remain unclear. In the Indian Ocean, notably two climate systems could have affected SST evolution during glacial and interglacial times: the annual cycle of the Indian Ocean monsoon system that stores and transfers heat and moisture between both hemispheres, and global climate changes via atmospheric teleconnection. Apparent discrepancies of last deglacial SST timing and magnitudes have also been observed among multiple SST studies (such as Mg/Ca, $U^{K'}_{37}$, and $TEX^{86}$) from the tropical western Indian Ocean, [*Bard et al*., 1997; *Caley et al*., 2011; *Kiefer et al*., 2006; *Levi et al*., 2007]. Records using $U^{K'}_{37}$ derived SST are marked by a two-step warming trend during the deglaciation that is broadly concomitant with the onset of Bølling-Allerød (B/A, ~14.6 ka) and the end of Younger Dryas (YD, ~12.5–11.5 ka) [*Bard et al*., 1997]. This supports that the regional SST evolution was synchronous with rapid climate changes occurring in the northern hemisphere during the last deglaciation [*Bard et al*., 1997]. In contrast, the SST records derived from planktonic foraminifera Mg/Ca and the foraminiferal modern analog technique indicate that the onset of the deglacial SST warming occurred earlier in apparent synchrony with Antarctic air temperature [*Kiefer et al*., 2006; *Levi et al*., 2007; *Naidu and Govil*, 2010]. The SST discrepancies support the notion that the timing of initial warming is contingent upon the proxy used to estimate the SSTs. In this perspective, SST reconstructions using multiple paleothermometry proxies may hold the key for understanding processes involved in shaping tropical SST records during terminations. A study based on multiple SST proxies from the Arabian Sea spanning the penultimate deglaciation indeed demonstrates clear discrepancies between two temperature recorders during the penultimate deglaciation [*Saher et al*., 2009]. However, this record was derived nearby the Somalia and Oman upwelling region, which may not be representative for the tropical Indian Ocean.

[4] Here we present SST records from a marine sediment core in the Mozambique Channel (core GIK 16160–3) of the planktonic foraminifera *Globigerinoides ruber* (*G. ruber* white) Mg/Ca and $U^{K'}_{37}$ together with records of $\delta^{18}O_{G.ruber}$ and ice volume corrected $\delta^{18}O_{seawater}$, The core was retrieved close to the Zambezi River mouth, providing sediment accumulation rates high enough to resolve the onset of the deglacial SST evolution with a multicentury temporal resolution. We consider the SST evolutions derived from two independent proxies in the same sedimentary sequence as a reflection of different season. Our goal is to reconcile the systematic differences observed in the absolute temperature estimates and timing of the onset of the deglacial SST warming in the tropical Indian Ocean.

## 2. Regional Hydrological Settings

[5] The Mozambique Channel displays a strong seasonal SST contrast of ~5°C between summer and winter. SST

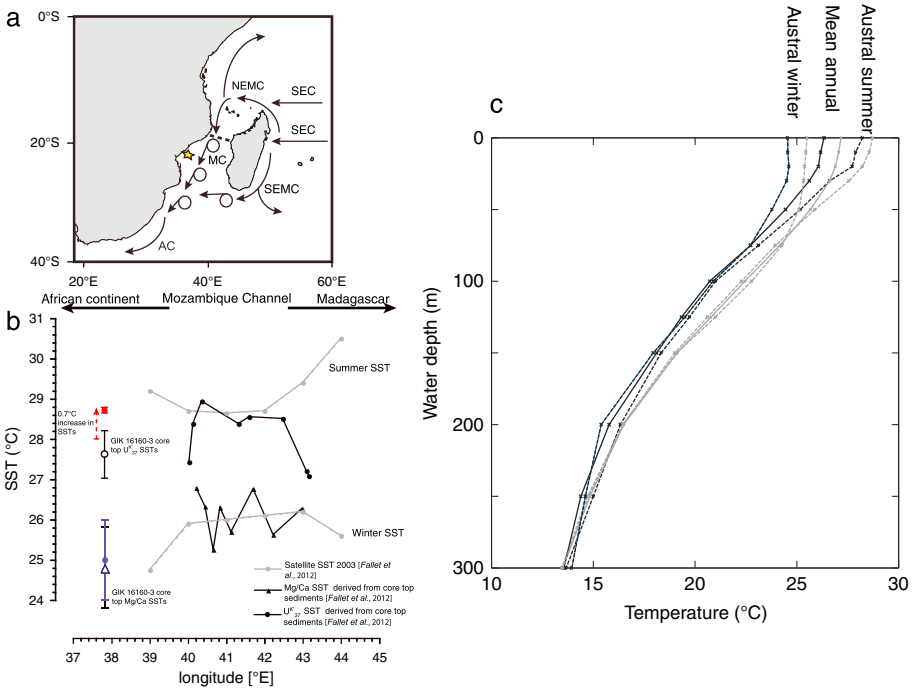


**Figure 2.** (a) The dominant currents in the Mozambique Channel and around Madagascar. AC: Agulhas Current; MC: Mozambique Current; SEMC: South East Madagascar Current; NEMC: North East Madagascar Current; SEC: Southern Equatorial Current. The star indicates core location. The dashed line between Madagascar and African continent represents the mooring transect from *Fallet et al*. [2012] shown in Figure 2b. (b) Variations of $U^{K'}_{37}$ and *G. ruber* Mg/Ca derived SST in surface sediments collected across the Mozambique Channel (data are after *Fallet et al*. [2012]). $U^{K'}_{37}$ SSTs were reestimated using *Songzoni et al*. [1997] for Indian Ocean core-top calibration. For comparison, summer and winter satellite SSTs (grey lines) are also plotted [*Fallet et al*., 2012]. The core-top SSTs derived from both $U^{K'}_{37}$ (open circle) and *G. ruber* Mg/Ca (open triangle) from GIK 16160–3 are also plotted together with satellite of SSTs summer (red circle) and winter (blue triangle) at our core site as well. (c) Water-column profiles of ocean temperatures for the upper 300 m at the core location of GIK16160-3 (black lines) and at mooring station 5A located at 16.8°S, 41.1°E, i.e., in the central part of the Mozambique Channel (grey lines) [*Fallet et al*., 2011] (data extracted from World Ocean Atlas 2001 [*Conkright et al*., 2002]). Solid lines illustrate annual mean temperatures, stippled lines austral summer, and winter temperatures. At mooring station 5A, *Fallet et al*. [2011] estimated the *G. ruber* habitat depth to about 20 m. Similarity of GIK16160-3 vertical temperature profile with mooring station 5A temperatures suggests *G. ruber*'s habitat depths to be similar.

minima of ~25°C occur in late austral winter (June–September), while maxima of ~30°C occur in austral summer (December–February), yielding an annual mean SST of ~27.6°C [*Fallet et al*., 2010] (Figures 1 and 2). There is also a distinct wet and dry season in western tropical Indian Ocean, which is concomitant with the SST annual cycle and its associated cross-equatorial heat and moisture advection (Figure 1). During wet season, prevailing northeasterly winds originating from northern tropics bring moisture from the tropical Indian Ocean to the African continent when SST maxima and its associated intertropical convergence zone (ITCZ) are situated in the Southern tropics. In contrast, the dry season is dominated by less humid southeasterly winds originating from the southern hemisphere midlatitudes as the SST maxima and the ITCZ are positioned in the northern tropics (Figures 1a and 1b).

[6] The Mozambique Channel is dominated by the discontinuous surface Mozambique Current (MC) that mainly constitutes of southward propagating anticyclonic eddies (Figure 2a). The MC is derived from the North East Madagascar Current (NEMC) [*New et al*., 2006], a branch of South Equatorial Current (SEC). These eddies, together with the South East Madagascar Current (SEMC) which constitutes another branch of SEC, transport tropical waters poleward and feeds into the Agulhas Current (AC), forming the upstream water source of the Agulhas leakage [*de Ruijter et al*., 1999 and Figure 2a].

[7] A recent study based on core-top sediments retrieved from the Mozambique Channel indicates that SSTs derived from $U^{K'}_{37}$ are warmer than those from *G. ruber* Mg/Ca [*Fallet et al*., 2012]. The warmer $U^{K'}_{37}$ SSTs closely resemble the austral summer temperature observed from satellite, while temperature estimates based on *G. ruber* Mg/Ca display colder values, which resemble the SST values of austral winter (Figures 2b and 2c). This observation suggests that different proxies in the Mozambique Channel are likely sensitive to different seasons, i.e., the $U^{K'}_{37}$ being skewed toward austral summer SSTs and the *G. ruber* Mg/Ca being skewed toward austral winter SSTs.

[8] Compared to the SSTs, the seasonal variation of sea surface salinity (SSS) in the Mozambique Channel is small, ranging from 34.8 psu during austral summer to 35.2 psu

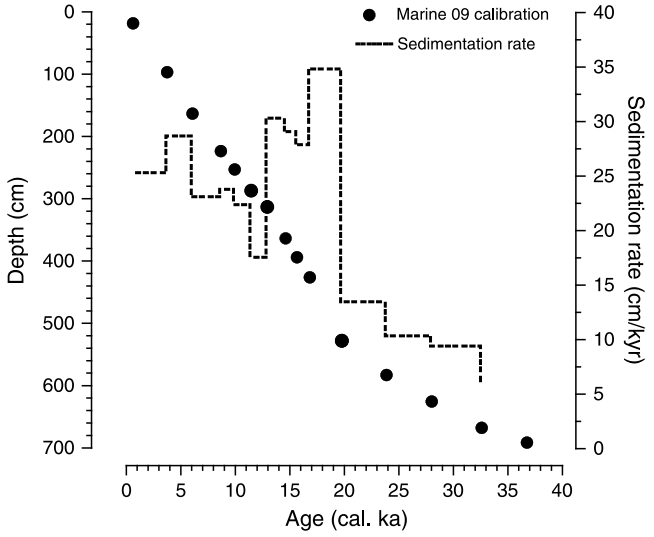


**Figure 3.** GIK16160-3 age model and sedimentation rate. The calendar age was calibrated using Marine 09 [*Reimer et al*., 2009].

during austral winter [*Fallet et al*., 2012]. However, the SSS field near the Zambezi River mouth is significantly influenced by river discharge during the wet season [*Siddorn et al*., 2001] compared to the main Mozambique Channel [*Fallet et al*., 2011].

## 3. Material and Methods

### 3.1. Core Descriptions and Age Control

[9] Core GIK16160-3 (18°14.47′S, 37°52.11′E, 1339 m water depth) was collected during R/V *Meteor Cruise 75/3 report*, 2008. The majority of the sediment consists of terrigenous olive gray sandy mud. There is an increase in sand content between 11 and 8 ka in the core, which is related to the flooding of the shelf break [*van der Lubbe et al*., 2012].

[10] Fifteen $^{14}$C-AMS dates were measured on mixed planktonic foraminifera fractions containing *G. ruber*, *G. trilobus*, and *G. sacculifer* at the Leibniz Laboratory for Radiometric Dating and Isotope Research, University of Kiel [*Wang et al*., 2013]. We converted $^{14}$C ages into calendar ages (Figure 3) using CALIB 6 program [*Stuiver and Reimer*, 1993] with the Marine09 calibration curve [*Reimer et al*., 2009] and have performed linear interpolations between radiocarbon dates. The detailed age model development is described elsewhere [*Wang et al*., 2013]. The 14 AMS dates reveal that core GIK 16160–3 covers the last 37 ka. A substantial increase in sedimentation rates occurs between ~19 and 12 ka compared to the full glacial and Holocene periods (Figure 3). This increase is probably resulting from a change in the modes of sediment delivery associated with changes in the Zambezi riverine runoff and/or with eustatic sea level rise [*van der Lubbe et al*., 2012].

### 3.2. $U^{K'}_{37}$ SST Temperature Estimates

[11] Alkenones were extracted from 1 g of homogenized bulk sediments and analyzed with double column gas chromatography at the Institute of Geosciences, University of Kiel (CAU). The analytical procedure of sample extraction and measurement on alkenones ($C_{37:3}$ and $C_{37:2}$) are fully described by *Rincon-Martinez et al*. [2010]. The $U^{K'}_{37}$ index was converted into SST using the calibration based on core-top sediments derived from Indian Ocean [*Sonzogni et al*., 1997] with a slope of 0.023 [*Bard et al*., 1997], because this calibration provides the best SST estimate for the 24°C–29°C temperature range for western Indian Ocean [*Bard et al*., 1997; *Sonzogni et al*., 1997]. Analytical precision based on duplicate analyses was always smaller than 0.015 $U^{K'}_{37}$ units, which is equivalent to 0.7°C [*Sonzogni et al*., 1997].

### 3.3. Foraminifera Mg/Ca Temperature Estimate and $\delta^{18}O$ Analyses

[12] The paired analyses of foraminiferal *G. ruber* Mg/Ca and $\delta^{18}O$ were performed on the same homogenized crushed samples (30–80 specimens) using a two-third split for Mg/Ca and a one-third split for $\delta^{18}O$ measurements. *G. ruber* was picked from the 250–315 μm size fraction. To prepare for Mg/Ca ratio analyses, we used a cleaning procedure including a reductive step [*Barker et al*., 2003]. The elemental analyses were performed on a Spectro Ciros SOP ICP OES with an external analytical error of ~0.1% at the Institute of Geosciences, CAU. Accuracy of the data was checked by analyzing the carbonate reference standard ECRM 752–1 [*Greaves et al*., 2008]. To convert Mg/Ca into temperature, we used the species-specific calibration equations with a given uncertainty of ±1.2°C for the 250–350 μm *G. ruber* size fraction [*Anand et al*., 2003]. To check reproducibility, we analyzed 18 out of a total of 140 samples in duplicates where each sample ranged within ±0.2°C, except one sample with an error of 0.6°C.

[13] The $\delta^{18}O_{G.ruber}$ was analyzed on a Kiel I (prototype) carbonate preparation device and a MAT 251 mass spectrometer at the Leibniz-Laboratory, CAU. Eighteen out of a total of 154 samples were run in duplicates with standard error of 0.035‰. The $\delta^{18}O_{seawater}$ values were calculated based on the paired measurements of $\delta^{18}O_{carbonate}$ and Mg/Ca-derived SST performed on *G. ruber* using the equation of *Bemis et al*. [1998]. We corrected for the effect of ice volume changes on $\delta^{18}O_{seawater}$ using the model simulation of *Bintanja et al*. [2005]. The residual ice-volume-corrected $\delta^{18}O_{seawater}$ ($\Delta\delta^{18}O_{seawater}$) reflects isotopic changes in local surface water that might be used as a proxy of local sea surface salinity [*Delaygue et al*., 2001]. Uncertainties of $\delta^{18}O_{seawater}$ estimates were obtained with an error propagation calculation of 1.2°C and 0.05‰ applying to SST estimates and $\delta^{18}O_{G.ruber}$ measurements, respectively, resulting in an overall uncertainty of ±0.26‰ (1σ), similar to the ±0.2‰ (1σ) estimated by *Rohling* [2007]. Assuming constant relationship between $\delta^{18}O_{seawater}$ and sea surface salinity (SSS) values at GIK 16160–3 coring site, we estimated SSS using the equation $\delta^{18}Osw = 0.49*Salinity-17.16$ published in *Fallet et al*. [2011].

[14] It has been repeatedly shown that calcite dissolution influences foraminiferal-based paleothermometry by preferentially removing $Mg^{2+}$ [*Brown and Elderfield*, 1996; *Dekens et al*., 2002; *Regenberg et al*., 2006], in contrast with diagenetic calcite precipitation that adds $Mg^{2+}$ [*Hoogakker et al*., 2009; *Regenberg et al*., 2007]. To examine potential impact of dissolution on foraminifera Mg/Ca, we report downcore weights of surface-dwelling planktonic foraminifera *G. trilobus* and *G. ruber* (supporting information Figure 1) and Scanning Electron Microscopy (SEM) photographs of *G. trilobus* (Figure 4). Before weighing, foraminifera were gently cleaned

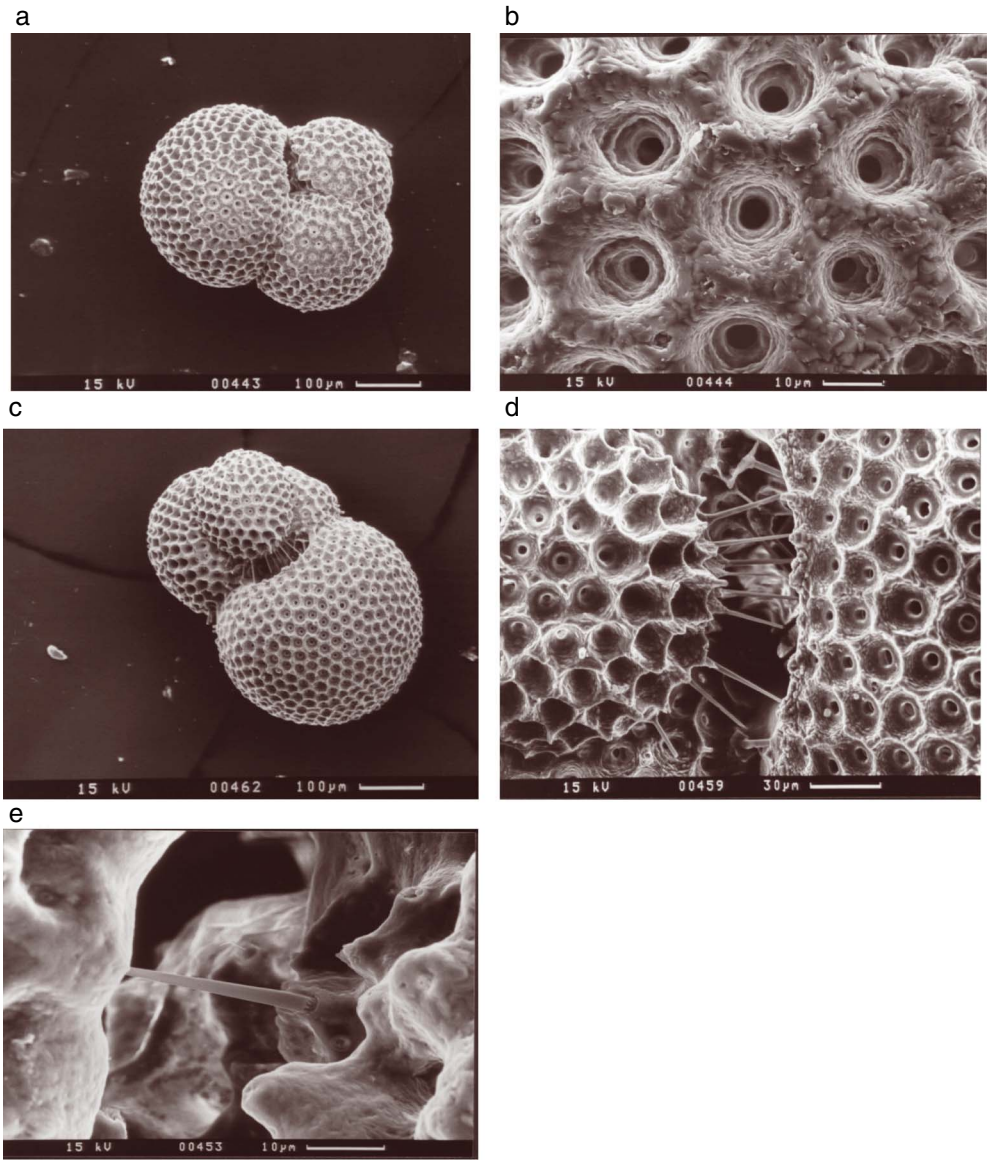


**Figure 4.** Scanning Electron Microscopy images of *G. trilobus* from GIK 16160–3 from (a and b) 468 cm; (c and d) 588 cm; and (e) 638 cm. Images from other depths also show no sign of dissolution.

by ultrasonication in demineralized water (three times) and ethanol (two times). We do not detect any discernable shift in planktonic foraminifera weights with age in the core (supporting information Figure 1). SEM photographs suggest remarkably well-preserved foraminifera tests with apparent spines, intact spine bases and ridges, and well-defined geometrical pores and interpore ridges (Figure 4), ruling out dissolution as a potential bias on Mg/Ca temperature estimates.

### 3.4. Model Validation on Seasonal SST Trends in the Mozambique Channel

[15] In order to examine winter and summer SST trends during the deglacial period, we extracted transient simulation results from the Atmosphere–ocean General Circulation Models (AOGCMs) of the climate evolution from the Last Glacial Maximum (LGM, ~21 ka) to 6 ka using the National Center for Atmospheric Research Community Climate System Model version 3 (NCAR CCSM3)) [*Liu et al*., 2009; *Shakun et al*., 2012]. The transient simulations were designed to recap all the abrupt climate events that occurred in response to various forcings during the last deglaciation [*Liu et al*., 2009; *He et al*., 2013]. Namely, the CCSM3 was set up with realistic changes in boundary conditions and forcing such as changes in insolation, atmospheric greenhouse gas concentrations, continental ice sheets, and coastlines from 21 to 6 ka [*Liu et al*., 2009; *Shakun et al*., 2012]. Details of the AOGCMs set up are fully described in *Liu et al*. [2009]. In the model simulation, meltwater flux was applied to the North Atlantic, Gulf of Mexico and the Southern Ocean using the scenario that produces the best agreement between the freshwater forcing and the history of sea level rise [*Liu et al*., 2009; *Shakun et al*., 2012]. Accordingly, freshwater fluxes were applied to the North Atlantic during the Heinrich Event 1 (HE1) and the Younger Dryas (YD) time intervals; a massive release within the southern hemisphere was used to account for the

contribution of the Antarctic ice sheet to the meltwater pulse 1A [*Deschamps et al*., 2012; *Liu et al*., 2009; *Shakun et al*., 2012]. As the simulation captures many major features of the deglacial climate evolution, including the magnitude of the climate response as inferred from paleostudies [*Liu et al*., 2009; *Shakun et al*., 2012], we anticipate that the model output would also capture the differences in seasonal SSTs at our coring site.

## 4. Results

### 4.1. $U^{K'}_{37}$ SSTs

[16] The $U^{K'}_{37}$ derived SSTs of GIK16160-3 varied between 24 and 28°C during the past 37,000 years (Figure 5c). The coldest $U^{K'}_{37}$ SST values were recorded between 19 and 14.6 ka, i.e., concomitant with the HE1, and match perfectly with the recently revisited estimation of the duration of the event [*Stanford et al*., 2011]. A wealth of $U^{K'}_{37}$ SST records revealed the extreme sensitivity to Heinrich events within the North Atlantic [e.g., *Bard et al*., 2000; *Pailler and Bard*, 2002; *Martrat et al*., 2007] (Figure 5b). This feature is not seen in the Greenland air temperature record, probably because Greenland temperature is mostly sensitive to sea ice shifts occurring during warming events [*Li et al*., 2005]. The coldest period in the North Atlantic SST records as well as in our core were likely induced by the total collapse of the North Atlantic Meridional Overturning Circulation (AMOC) as recorded in the $^{231}Pa/^{230}Th$ during HE1 [*McManus et al*., 2004] (Figure 5b). This suggests that our $U^{K'}_{37}$ SST is closely linked to rapid climate change in the Northern hemisphere. The $U^{K'}_{37}$ SST then abruptly increased by 1.6°C at ~15 ka, i.e., at the onset of the Bølling-Allerød (B/A) chronozone (Figure 5c), mimicking the rapid temperature shifts observed in Greenland ice core (Figures 5a and 5c). For Younger Dryas (YD), there is no apparent synchrony between our SST record and the North Atlantic SST [*Bard et al*., 2000] as well as the slowdown of the AMOC [*McManus et al*., 2004] (Figures 5b and 5c). This lack of synchrony is also corroborated by another $U^{K'}_{37}$ SST record from the adjacent core MD 79257 [*Bard et al*., 1997 and supporting information Figure 2]. Rather being synchronous with climate records from the North Atlantic realm, the YD in the southwestern Indian Ocean was marked by a slight warming trend (Figure 5c). Furthermore, the $U^{K'}_{37}$ SSTs in the Mozambique Channel [*Bard et al*., 1997 and this study] did not reach its warmest temperature until the middle Holocene, pointing to a lack of perfect match between $U^{K'}_{37}$ SST records from the North Atlantic and the southwestern tropical Indian Ocean during the second half of the deglaciation (Figures 5b and 5c).

### 4.2. Foraminifera Mg/Ca-derived SST, $\delta^{18}O_{G.ruber}$, and $\Delta\delta^{18}O_{seawater}$

[17] The Mg/Ca of surface-dwelling species *G. ruber* ranged between 3.2 and 4.3 mmol/mol, with the uppermost Mg/Ca values in core GIK 16160–3 in agreement with modern core-top *G. ruber* values in Mozambique Channel [*Fallet et al*., 2012]. Mg/Ca-derived SST estimates range between 22 and 25°C. The magnitude of temperature variability in our Mg/Ca SST record and the initial timing of temperature rise are in broad agreement with other regional Mg/Ca SST records [*Kiefer et al*., 2006, *Naidu and Govil*, 2010; *Saraswat et al*., 2013]. In particular, the Mg/Ca record (Figure 5d) displays an early warming starting at ~18 ka, which is synchronous with the onset of the Antarctic air temperature rise during the deglaciation within the age model uncertainties (Figure 5e). Mg/Ca SSTs increased almost to the modern values during the HE1 when the $U^{K'}_{37}$ SSTs are coldest (Figures 5c and 5d). During the second half of the deglaciation, a series of multicentury SST fluctuations with a magnitude lower than 1°C are also observed and seem to generally match to the Antarctic temperature record (Figures 5d and 5e). Interestingly, a warming period is recorded during the YD, which is in phase with Antarctic temperatures and mimics the $U^{K'}_{37}$ SST record.

[18] The gradual decrease in the $\delta^{18}O$ record derived from *G. ruber* is concomitant with the deglacial warming trend recorded in the $\delta^{18}O$ of the EPICA Dronning Maud Land (EDML) ice core and Mg/Ca SST record (Figures 5e and 5f). The $\delta^{18}O$ value of −2.22‰ in the uppermost part of the core falls within the $\delta^{18}O_{G.ruber}$ range obtained from a modern survey of the core-top sediments in the Mozambique Channel [*Fallet et al*., 2012]. The computation of $\Delta\delta^{18}O_{seawater}$ yields variations of 0.8 (±0.2)‰ during the last 37,000 years, with positive anomalies recorded during the HE1 and negative ones during the Glacial and the Holocene periods (Figure 5g). The estimated SSS based on $\Delta\delta^{18}O_{seawater}$ demonstrates small salinity variations, ranging between 33.8 and 35.1 psu. The topmost salinity value from our core is 34.3 psu, which resembles the modern value of 34 psu observed near the Zambezi River mouth [*Siddorn et al*., 2001].

## 5. Discussion

### 5.1. Discrepancies in $U^{K'}_{37}$ and Mg/Ca SST Records

[19] We observe discrepancies in both magnitudes and timing of deglacial warming between the SST records of $U^{K'}_{37}$ and *G. ruber* Mg/Ca. The only similarity of the two SST records is that both records indicate a Last Glacial Maximum (LGM) cooler than the present by 3 to 4°C (Figures 5c and 5d), which is in agreement with previously estimated SSTs in the region [*Bard et al*., 1997; *Sonzogni et al*., 1997; *Kiefer et al*., 2006; *Caley et al*., 2011, MARGO, 2009]. The absolute $U^{K'}_{37}$ SSTs for the last 37,000 years are higher than the Mg/Ca-derived SSTs by 2 to 4°C, except during the HE1, 14.3–13.6 ka, and 11.5–10.6 ka. During the HE1, the $U^{K'}_{37}$ and Mg/Ca SSTs are essentially the same (Figures 5c and 5d). The 2 to 4°C temperature difference is too large and systematic to be explained by the choice of the paleotemperature calibration equations. The uncertainty of the $U^{K'}_{37}$ SST estimates based on modern core-top sediment calibration from the western tropical Indian Ocean ranges within a confidence interval of ± 0.7°C [*Sonzogni et al*., 1997]. Our SST estimates based on *Sonzogni et al*. [1997] would be very similar to those based on the most recent global core-top calibration with uncertainty of 0.6°C from *Conte et al*. [2006]. The uncertainty of Mg/Ca-SST estimates is about ±1°C regardless of whether an exponential [*Anand et al*., 2003] or a linear equation is used [*Fallet et al*., 2010]. This confidence interval is slightly larger than those associated with alkenone-based estimates. However, measurement uncertainties of 0.7°C for $U^{K'}_{37}$ or 1.2°C for Mg/Ca of the *G. ruber* cannot explain the up to 4°C SST offset between alkenone and Mg/Ca paleothermometers. Furthermore, large SST offsets

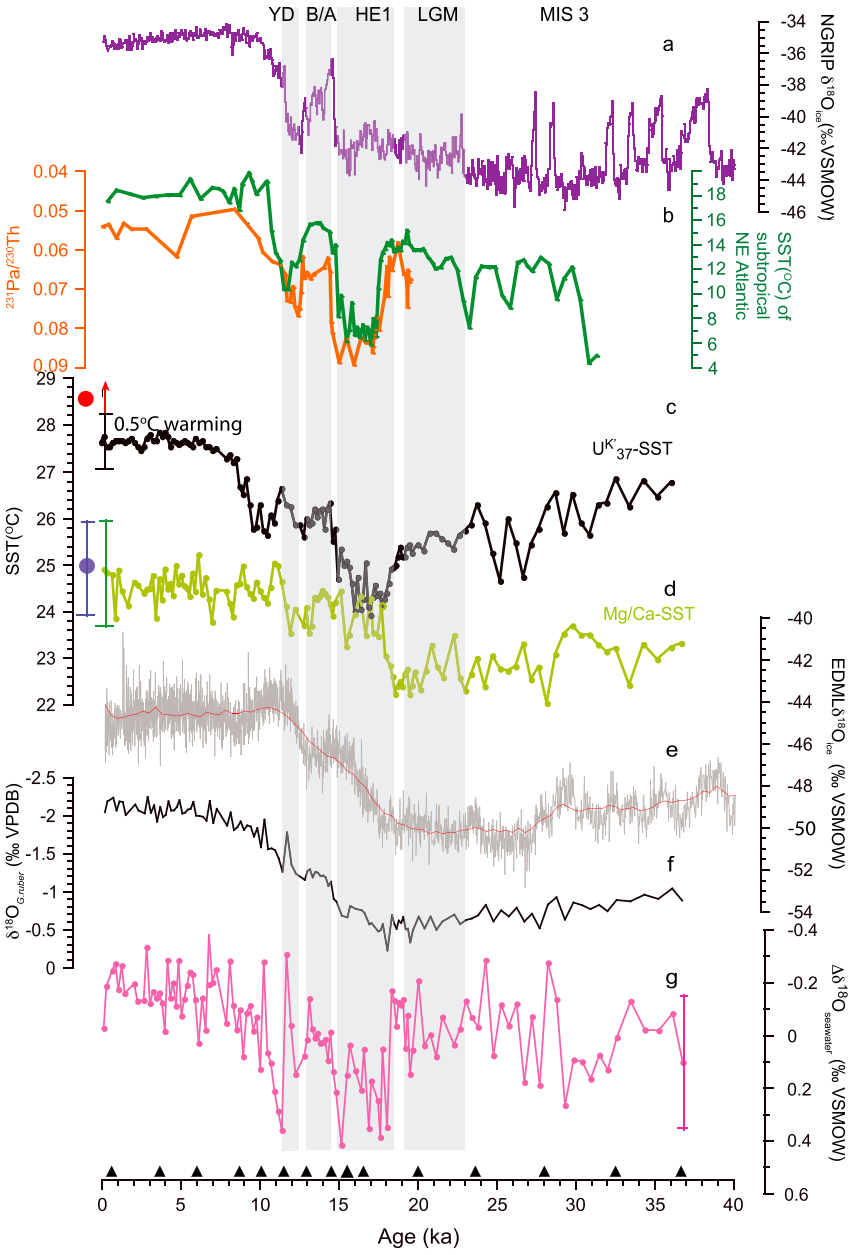


**Figure 5.** Records of GIK16160-3 versus age for the last 37,000 years in comparison with ice core records from Greenland and Antarctica. (a) Variations in air temperatures over Greenland indicated by $\delta^{18}O$ record of NGRIP ice core [*NGRIP-members*, 2004]; (b) Sedimentary $^{231}Pa/^{230Th}$ (orange line) as a kinematic proxy for the meridional overturning circulation from subtropical North Atlantic Ocean [*McManus et al*., 2004] and reconstructed $U^{K'}_{37}$ SST record from subtropical Northeast Atlantic [*Bard et al*., 2000]; (c) $U^{K'}_{37}$ derived SSTs; (c) *G. ruber* Mg/Ca derived SSTs; (d) Variations in air temperatures over Antarctica indicated by $\delta^{18}O$ record from EPICA-Dronning Maud Land ice core and the thin red line represents the smoothed EDML $\delta^{18}O$ [*Epica-Community-Members*, 2006]; (e) *G. ruber* $\delta^{18}O$ record; (f) Ice volume corrected $\Delta\delta^{18}O_{seawater}$ record, and the error bar (1σ of ±0.26‰) for $\Delta\delta^{18}O_{seawater}$ are also plotted. The black triangles show calibrated calendar age based on the measured AMS $^{14}C$ dates. Relevant chronozones are shaded in grey: YD, Younger Dryas (~12.5–11.5 ka); HE1, Heinrich Event 1 (~19–14.6 ka); LGM, Last Glacial Maximum ~23–19 ka); and MIS 3, marine isotope stage 3. The blue dot is the modern winter temperature and the red dot is the modern summer temperature (1960–2002, http://nomads.ncdc.noaa.gov/thredds/dodsC/). The red arrow indicates recent 0.5–0.7°C warming in tropical Indian Ocean.

(up to 3°C) between the two proxies are also independently observed in core-top sediments [*Fallet et al*., 2012] as well as at glacial/interglacial timescales in the Mozambique Channel [*Caley et al*., 2011; *Saher et al*., 2009]. These observations suggest that warmer $U^{K'}_{37}$ SSTs and cooler Mg/Ca SSTs are robust features in the western tropical Indian Ocean.

[20] The timing of initial warming observed in $U^{K'}_{37}$ and Mg/Ca-based SST records during the deglaciation also differs significantly, further suggesting that both proxies do not record the same oceanic characteristics. The magnitude of temperature changes and overall trends from our $U^{K'}_{37}$ SST record agree remarkably well with a previous $U^{K'}_{37}$ SST record [*Bard et al*., 1997] from an adjacent core of MD 79275 (Figure 1 and supporting information Figure 2) in the Mozambique Channel. Both cores show a rapid warming at the onset of the B/A, synchronizing the rapid temperature shifts observed in Greenland ice core. Hence, our $U^{K'}_{37}$ SST fully supports the notion that the timing of $U^{K'}_{37}$ SST in the southwestern Indian Ocean at the onset of the deglaciation is in synchronicity with millennial-scale climate fluctuations in the northern hemisphere [*Bard et al*., 1997]. In contrast, the initial warming recorded in Mg/Ca ratios of *G. ruber* from tropical Indian Ocean at the onset of the deglaciation occurs much earlier than that of alkenone records [*Kiefer et al*., 2006; *Naidu and Govil*, 2010; this study], and appears to be synchronous with Antarctic air temperature rise (Figure 5).

### 5.2. Controls on the Differences in SST Records

[21] The robustness of the SST offset (up to 4°C) between the two proxies observed in Mozambique Channel [*Caley et al*., 2011; *Fallet et al*., 2012; this study] suggests that a persistent mechanism was responsible for these discrepancies. In the following discussion, we argue that the warmer $U^{K'}_{37}$ than Mg/Ca SST is a pervasive feature for our core location, which is tied to contrasting seasonal characteristics at a regional scale rather than postdepositional processes or sedimentary biases.

[22] Multiple evidences from our core suggest that no dissolution has influenced Mg/Ca values in the sediments (Figure 4 and supporting information Figure 1). In particular, planktonic foraminifera weights (supporting information Figure 1) throughout the core are within the weight ranges of modern specimens observed from core tops and sediment traps in the Mozambique Channel [*Fallet et al*., 2012]. According to the SEM photographs, recrystallization is also unlikely (Figure 4). Additionally, *G. ruber* $\delta^{13}C$ shows typical glacial-interglacial changes with minimum values of ~0.4‰ (supporting information Figure 3), one value much too high to be explained by syn-sedimentary recrystallization of pore water $\delta^{13}C$ with negative $\delta^{13}C_{DIC}$ [*McCorkle et al*., 1985; *Blanchet et al*., 2012]. Rather, these *G. ruber* $\delta^{13}C$ shifts can be linked to changes in the global oceanic $\delta^{13}C$ of the $\Sigma CO_2$ pool, which are triggered by changes in the terrestrial biosphere [*Shackleton*, 1977]. We hence rule out any potential bias associated with dissolution and/or recrystallization of foraminifera tests in the Mg/Ca SST estimates.

[23] We also rule out that salinity changes affected Mg/Ca values in our core. Salinity can significantly affect Mg/Ca ratios when it is higher than 35 psu [*Arbuzewski et al*., 2010], but it does not impact $U^{K'}_{37}$ values for the range of salinities encountered in low latitudes [*Herbert*, 2001; *Sonzogni et al*., 1997]. The topmost salinity value in our core is about 34.4 psu, which closely resembles the modern value of ~34 psu near the Zambezi River mouth [*Siddorn et al*., 2001]. Also, the salinity for the rest of the core was lower than 35 psu except for 35.1 psu during HE1. A salinity correction for HE1 based on *Kisakürek et al*. [2008] would lower Mg/Ca ratios, consequentially resulting in 0.6 to 0.8° C lower temperature estimates. Such correction would not change the overall SST trend recorded during HE1. Furthermore, the magnitude of ~3°C increase in Mg/Ca SST from the LGM to the Holocene agrees with previous studies in the region and elsewhere in the tropics [*Bard et al*., 1997; *Caley et al*., 2011; *Kiefer et al*., 2006; *MARGO*, 2009], further supporting that salinity only had a negligible effect on Mg/Ca values at our core site, despite its proximity to the Zambezi estuary.

[24] Bioturbation also could not explain the large discrepancies between the two SSTs embedded in different particle size fractions of coccolithophorids and foraminifera. For cores with sedimentation rates smaller than 10 cm/kyr, bioturbation can cause age discrepancies of up to 3 kyr [*Bard*, 2001]. In our core, sedimentation rates are much higher than 10 cm/kyr during the deglaciation (Figure 3) with the highest sedimentation rate reaching ~35 cm/kyr during HE1, when the two SST records of two proxies diverge the most. In fact, the alkenone cooling occurring synchronously with the Mg/Ca warming is documented by 16 data points dated between 19.6 ka and 17.2 ka. It corresponds to a sedimentary depth interval thicker than 80 cm, i.e., an order of magnitude thicker than the bioturbational mixing depth [*Trauth et al*., 1997]. Thus, we conclude that the sedimentation rates are too high to have any significant impact on SST estimates through phase shift and signal attenuation carried by different size fractions [*Bard*, 2001].

[25] It is generally assumed that the finer particles are more prone to lateral advection and resuspension as compared to the tests of planktonic foraminifera, which may result in significantly older $^{14}C$ ages for alkenones than foraminifera and affect alkenone temperature records [*Mollenhauer et al*., 2003; *Mollenhauer et al*., 2005; *Ohkouchi et al*., 2002; *Sicre et al*., 2005]. To our knowledge, no radiocarbon dating on alkenones has been performed within the region; however, in a sediment core-top study from Mozambique Channel, *Fallet et al*. [2012] measured $^{14}C$ ages of both total organic carbon (TOC) and *G. ruber* on two samples. They found the uncalibrated $^{14}C$ age differences being 80 and 280 years younger on TOC than on *G. ruber*, suggesting that organic material being delivered in that region being a mixture of fresh marine and terrestrial compounds. Indeed, a substantial fraction of TOC at Zambezi River mouth is of terrigenous origin [*Wang et al*., 2013]. We hence conclude that according to the data currently available lateral transport or resuspension of significantly older alkenones did not occur at our core location.

[26] Ultimately, differences in habitat depth of alkenone-producing coccolithophorids and *G. ruber* can also result in SST differences recorded by Mg/Ca and $U^{K'}_{37}$ paleothermometry if these planktons dwell below the surface mixed layer [*Mix*, 2006]. *Fallet et al.* [2011], however, estimated that *G. ruber* and alkenone-producing coccolithophorids both live within the upper water column, and have a similar habitat depth of ~0 to 20 m in the middle of Mozambique Channel. At our core location by the Zambezi river mouth the vertical temperature structure of upper water at different seasons is very similar to that

in the middle of the Channel with a consistent 1°C offset (Figure 2c). This suggests that coastal processes have negligible effects on the season and habitat depth at our core location. The core-top alkenone and Mg/Ca-derived SST values perfectly match the ones found at the corresponding sites for summer and winter SST, respectively (Figures 2b, 5c, and 5d). Although *G. ruber* records colder SSTs than the alkenone-producing coccolithophorids (Figures 2b, 5c, and 5d), it is highly unlikely that *G. ruber* records subsurface water temperatures. *G. ruber* possesses photosymbiotic algae that need sufficient light and hence restrict *G. ruber* to be most productive within the euphotic zone [*Birch et al*., 2013 and references therein]. Also, *G. ruber* has recently been reported to live in water depths shallower than 25 m in the western tropical Indian Ocean [*Fallet et al*., 2011; *Friedrich et al*., 2012; *Birch et al*., 2013]. If *G. ruber* had recorded the mean-annual or summer temperature, this would then require this species lived in water depths below 50 m (Figure 2), which contradicts any current understanding of *G. ruber* habitat depth [*Fallet et al*., 2011; *Friedrich et al*., 2012; *Birch et al*., 2013].

### 5.3. Different Seasonal Effects on the Proxy-Based SST Estimates

[27] None of mechanisms discussed above can adequately explain the differences in the proxy-dependent contrasts in SST absolute values and trends at the core site. These contrasting SST trends are therefore likely to reflect different hydrological conditions at the regional scale. The fact that $U^{K'}_{37}$ and *G. ruber* Mg/Ca SSTs from core top in the Mozambique Channel resemble the satellite observed austral summer and winter temperature, respectively, supports that each SST proxy is skewed toward a different season (Figure 2). Our Mg/Ca value of 4.3 mmol/mol in the topmost sediment is indeed closer to the modern winter value of 3.8 mmol/mol than to the summer value of 6.2 mmol/mol [*Fallet et al*., 2010], suggesting that the core-top Mg/Ca SSTs tracks temperature recorded during austral wintertime. Such core-top values translate into SST values of 24.8 ± 1.2°C, which is identical to modern winter SST value of 25.0 ± 1.0°C (1960–2002, http://nomads.ncdc.noaa.gov/thredds/dodsC/). Likewise, the topmost $U^{K'}_{37}$ SST estimate of 27.6 ± 0.6°C is more similar to the mean modern summer SSTs of 28.7 ± 0.1°C (1960–2002, http://nomads.ncdc.noaa.gov/thredds/dodsC/) given that the SST has increased up to 0.7°C in the tropical Indian Ocean over the last five decades [*Du and Xie*, 2008; *Kothawale et al*., 2008].

[28] We hypothesize that $U^{K'}_{37}$ and *G. ruber* Mg/Ca preferentially record seasonal SSTs that are above and below the annual mean SSTs, respectively. Alkenone-producing coccolithophorids growing period peaks during the warm season (December–February) in the southwestern Indian Ocean [*Raj et al*., 2010]. Sediment traps deployed during 2003–2006 corroborated that summer months are the peak season for alkenone concentrations although flux-weighted SSTs closely reflect mean-annual SST values [*Fallet et al*., 2011]. This is probably due to the fact that the $U^{K'}_{37}$ index reached the value of 1 during summer months [*Fallet et al*., 2011]. Also, *G. ruber* fluxes collected by sediment traps indicate that this species mostly peaks during summer months as well but they record mean-annual temperature instead of summer temperature [*Fallet et al*., 2010]. However, comparison of Mg/Ca-based SST between mooring traps and core-top sediment from the same area suggests that Mg/Ca SST estimates from core-top sediment are colder by up to 3°C than those from sediment traps [*Fallet et al*., 2012]. This temperature difference is too large to be explained by the recent warming of up to 0.7°C in Indian Ocean [*Du and Xie*, 2008; *Kothawale et al*., 2008] or the Mg/Ca SST variability during the Holocene (Figure 5d). As no dissolution is detected in surface sediment [*Fallet et al*., 2011; this study], this temperature offset suggests that mooring trap only captures a temporal snapshot of bloom conditions during 2003–2006 in the Mozambique Channel, and does not reflect the season-weighted SST that is captured in the sediments on multidecadal timescales [*Fallet et al*., 2010]. Indeed, unlike sediment traps, core-top samples integrate the entire life cycle of *G. ruber* that will eventually form the sedimentary signal. Hence, core-top samples reflect the full spectrum of SST recorded by *G. ruber* on multidecadal timescales more accurately than sediment traps.

[29] An eco-physiological growth rate model for the most abundant planktic foraminifer species living in the ocean surface and subsurface waters suggests that *G. ruber* peaks at a different season than alkenone-producing coccolithophorids in our core study site [*Lombard et al*., 2011]. This model, which is well suited for reflecting seasonality, predicts that that the maximum annual productivity of *G. ruber* in the Mozambique Channel occurs during austral spring (i.e., October and November) in the top 20 m water column [*Lombard et al*., 2011]. Thus, a season- and depth-weighted Mg/Ca-derived temperature will be representative of the upper mixed layer, but skewed toward seasons when temperature is below the mean-annual SST (A. Lombard, personal communication). Another planktonic foraminifera model based solely on the modern spatial distribution of *G. ruber* also predicted that calcification temperature in the Mozambique Channel occurs during a period of the year when SST is below the mean-annual SST [*Fraile et al*., 2009a]. We can of course not rule out a possible shift in the seasonal preference of *G. ruber* and alkenone producers through time, as it can be triggered by oceanographic and climatic changes while applying SST proxies back in time [*Lohmann et al*., 2012]. However, model simulations by *Fraile et al*. [2009b] suggest that compared to present day there was no shift in seasonal maximum *G. ruber* flux in the tropical southwestern Indian Ocean during the last glacial maximum. When the latter model is tuned to LGM boundary conditions, it suggests that our hypothesis of a constant seasonality for *G. ruber* is valid at our core location [*Fraile et al*., 2009b]. We know of no other mechanism than seasonality by which to reconcile the differences between the two SST records throughout the studied time interval (Figure 6). We hence interpret the $U^{K'}_{37}$ and the *G. ruber* Mg/Ca as reliable temperature indicators of warm season (summer) and cold season (winter/spring), respectively, and assume that this seasonal pattern has not changed through time.

### 5.4. Underlying Mechanism for Different Seasonal SST Records

[30] Our study suggests that the seasonal southwestern tropical Indian Ocean SSTs were closely linked to climate changes occurring in both hemispheres. The annual cycle of SST in turn determines the monsoonal wind direction and its associated changes in the area where advection of heat

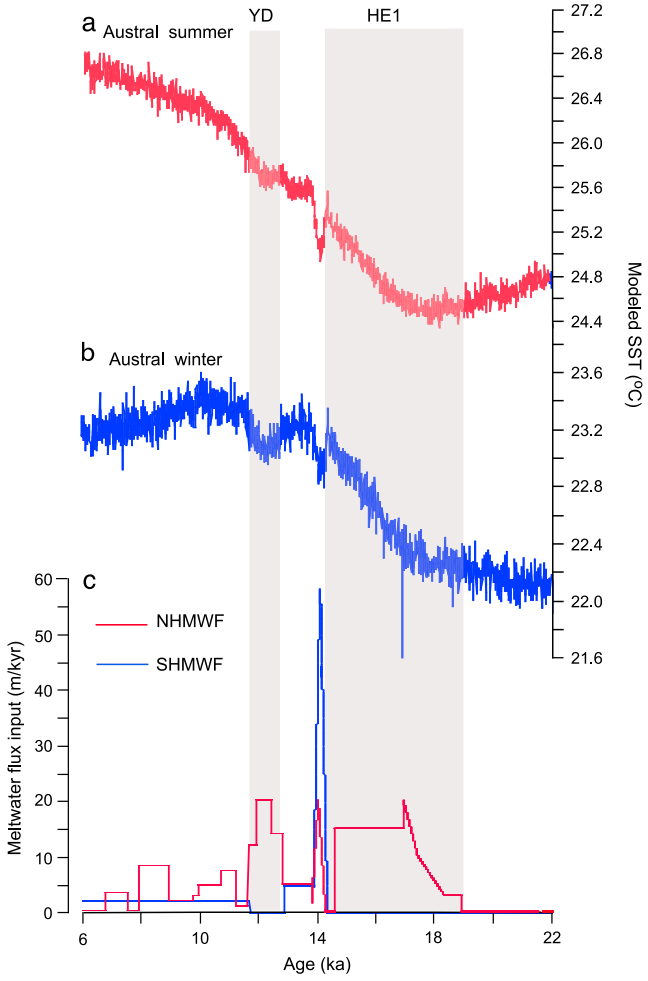


**Figure 6.** Model output of (a) transient austral summer and (b) winter SSTs for the Mozambique Channel; (c) Melt water fluxes for both Northern Hemisphere and Southern Hemisphere derived from CGCM3 model [*Liu et al*., 2009; *Shakun et al*., 2012].

and moisture impacts rainfall amount in tropical Africa, and latitudinal movement of the ITCZ (Figure 1). Owing to the seasonal positions of SST maxima from austral summer to winter, the western tropical Indian Ocean is alternately situated in the northern and southern meteorological hemispheres through interhemispheric displacements of the ITCZ, respectively (Figure 1). As a result, our core location is situated north of the meteorological equator when the warm and humid northeasterly winds prevail and the ITCZ shifts to its southernmost position (Figure 1a). This may explain that the $U^{K'}_{37}$ SSTs have strong affinity with the temperature changes recorded in the Northern Hemisphere, in particular during the HE1 [*Bard et al*., 1997; this study]. On the other hand, the SST pattern recorded by Mg/Ca ratios of *G. ruber* during the HE1 indicates that cold season SSTs were predominantly mimicking the Antarctic temperature record at the onset of the last deglaciation [*Kiefer et al*., 2006; *Naidu and Govil*, 2010; this study]. This can probably be explained by the fact that the ITCZ shifts to its northern position during austral winter, making our core site situated in the southern meteorological hemisphere. Consequently, the core location was influenced by the cool and dry southeasterly winds originating from southern hemisphere midlatitudes during austral winter (Figure 1b). Cold season temperatures recorded by *G. ruber* Mg/Ca are in full agreement with the recent reinterpretation of Antarctic temperature records as reflecting winter temperatures [*Laepple et al*., 2011]. We therefore argue that the annual cycle of SST maxima and prevailing wind directions above the coring site are plausible underlying mechanisms to explain why the northern or southern hemispheres were both recorded in our marine records. Such feature might be most obvious during HE1, when the cooling in the Northern Hemisphere resulted in an extreme weakening of the AMOC [*McManus et al*., 2004] along with a prominent southward shift of the ITCZ [*Denton et al*., 2010], when seasonality virtually vanished at our study site (Figure 6).

[31] Our hypothesis of seasonal SST dominance in the individual paleothermometers is further supported by one transient simulation of Termination 1 performed using coupled atmosphere–ocean general circulation models (AOGCMs) [*Liu et al*., 2009; *Shakun et al*., 2012, *He et al*., 2013]. The AOGCMs output for the Mozambique Channel (16°S, 39°E) indicates that the deglacial austral winter SST warming trend was leading that of the austral summer SST at the onset of the deglaciation by ~2.5 kyr (Figures 6a and 6b). Although the simulation does not reach the magnitude of SST rise seen in proxy data, the different timings of initial warming for winter and summer perfectly reflect the Southern and Northern Hemisphere deglacial SST trends, respectively (Figure 6). The sequence of short-lived warm and cold intervals within the simulated SST mediated by freshwater flux in the North Atlantic mimics the interhemispheric bipolar seesaw during the HE1 [*Liu et al*., 2009; *Shakun et al*., 2012]. The coldest austral summer SSTs simulated at our core location coincide with surges of meltwater in the Northern Hemisphere that occurred at the onset of HE1 (Figure 6c). Furthermore, both simulated summer SST [*Liu et al*., 2009] and $U^{K'}_{37}$ SST trends in our core location [*Bard et al*., 1997; this study] show a two-step warming, in phase with SST trends recorded in the Northern Hemisphere but lagging behind initial deglacial warming in the Southern Hemisphere [*Shakun et al*., 2012]. This confirms that summer SSTs derived from $U^{K'}_{37}$ in tropical Indian Ocean were paced by Northern Hemisphere Climate during the deglaciation. In contrast, both simulated winter SST [*Liu et al*., 2009] and Mg/Ca SST records [*Caley et al*., 2011; *Kiefer et al*., 2006; *Naidu and Govil*, 2010; *Saraswat et al*., 2013; this study] show steady warming already during HE1, in agreement with SST trends of Southern Hemisphere temperatures [*Shakun et al*., 2012]. This further supports that the deglacial SST derived from *G. ruber* Mg/Ca during austral winter at our core site was influenced by Antarctic climate. The agreement between our data and the transient model [*Liu et al*., 2009] suggests that both proxies provide accurate estimate of timing and magnitudes of changes in seasonal SST variations, further supporting that the tropical Indian Ocean SST was closely linked to both hemisphere's climate changes.

[32] The simulated temperature by AOGCMs decreased less than 0.2°C during the YD, which is not observed in our SST records (Figures 5 and 6). This might reflect inherent limitations of models to capture the regional seasonal SST changes during the YD (Figures 5 and 6). One would expect the SST changes observed at our core location to depict similar opposite temperature shifts as observed during the HE1 if the seasonal ITCZ dynamics was comparable to that

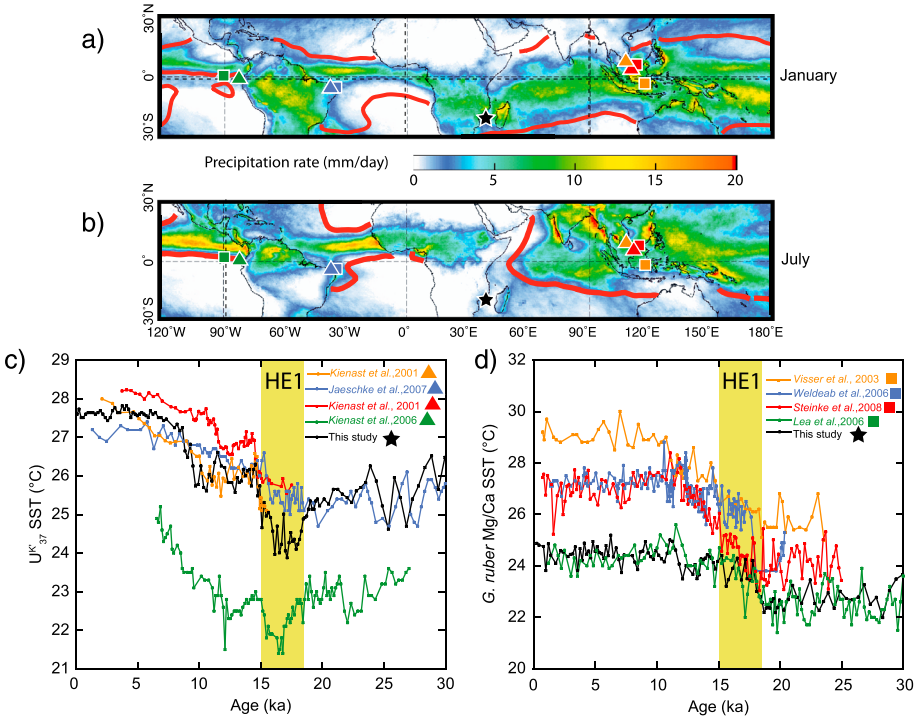


**Figure 7.** Upper panels: Modern-day (a) January and (b) July precipitation rates estimated from satellite imagery of the Tropical Rainfall Measuring Mission (http://trmm.gsfc.nasa.gov/). Red bands indicate the 26°C isotherm according to World Ocean Atlas 2001 [*Conkright et al.*, 2002]. Squares indicate core locations for Mg/Ca records and triangles indicate core locations for alkenone records shown in the lower panels. Black star indicates GIK16160-3 core location. Lower panels: examples of alkenone records (c) compared to Mg/Ca records (d) of deglacial SST estimates from tropical oceans. We have recalibrated all these published records using marine 09 to be consistent with the age model established for core GIK16160-3. We applied the reservoir corrections used by the original authors. Reservoir corrections were assumed to be 400 years if not otherwise stated in the original publications. The green vertical bar indicates the HE1 chronozone.

observed during the HE1. That both SST proxies show a transient warming trend matching to the Antarctic temperature record suggest both seasons were under the influence of the southern hemisphere climate dynamics. It implies that the ITCZ position was located north of our core location during that time interval, which goes against the notion that ITCZ southward shifts occur during North Atlantic cold spells such as the YD [*Gasse et al.*, 2008 and reference therein]. A deglacial rainfall record from Socotra Island, however, confirms that the YD chronozone was as wet as the B/A [*Shakun et al.*, 2007]. This suggests that the southward shift of the ITCZ was not as prominent during the YD as compared to the HE1.

[33] Our records corroborate SST mismatches recorded by different temperature proxies during the penultimate interglacial period in the Arabian Sea [*Saher et al.*, 2009], suggesting the seasonal effects on SSTs are a pervasive feature in the western tropical Indian Ocean during terminations. In addition, our hypothesis also explains discrepancies in SST records for deglacial timing and absolute temperature values that have been recorded in the tropical Indian Ocean [*Bard et al.*, 1997; *Caley et al.*, 2011; *Kiefer et al.*, 2006; *Naidu and Govil*, 2010; *Saraswat et al.*, 2013; this study]. Beside the western Indian Ocean, a synthesis of deglacial SST records highlights such discrepancies at other tropical locations. These sites include the western equatorial Atlantic [*Weldeab et al.*, 2006; *Jaeschke et al.*, 2007], eastern, and western Equatorial Pacific [*Lea et al.*, 2000; *Lea et al.*, 2006; *de Garidel-Thoron et al.*, 2007; *Kienast et al.*, 2001; *Linsley et al.*, 2010; *Rosenthal et al.*, 2006; *Steinke et al.*, 2008; *Visser et al.*, 2003] (Figure 7). Another study also documents the contrasting cooling and warming trends registered in alkenones and Mg/Ca during HE1 from the same marine core derived from South of Sumatra in the eastern Indian Ocean [*Mohtadi et al.*, 2010].

[34] Discrepancies between deglacial SST records were first recognized in the Eastern Equatorial Pacific (EEP) [*Mix*, 2006; *Kienast et al.*, 2006; *Pahnke et al.*, 2007; *Lea et al.*, 2006; *Koutavas and Sachs*, 2008]. SST records derived from $U^{K'}_{37}$ in the EEP generally support the view that changes in the AMOC were instrumental in determining temperature evolution in the tropics [*Kienast et al.*, 2006; *Pahnke et al.*, 2007] suggesting that tropical SSTs were responding to climate change occurring in the Northern hemisphere. On the other hand, Mg/Ca SST records highlight an early SST warming that might have preceded changes in continental ice sheets during the last deglaciation [*Lea et al.*, 2000; *Lea et al.*, 2006] supporting the viewpoint that deglaciations are mainly driven by climatic processes occurring in the Southern hemisphere or the tropics. Our interpretation of

seasonal SSTs offers an alternative view in that tropical SST evolution during deglacial terminations could have been influenced by climate from both hemispheres. It clearly remains to be understood why our seasonal SST hypothesis may apply to the tropical ocean as a whole since mismatches of alkenones and Mg/Ca SSTs during terminations provide coherent signals regardless the hemisphere (Figure 7). It also needs to be further investigated whether the observed SST trends from both proxies during HE1 applies for other Heinrich events.

### 5.5. Implication of SST Seasonality for Agulas Leakage during the Deglacial

[35] The early warming recorded in *G. ruber* Mg/Ca SSTs provides insights into the mechanisms responsible for the seasonal SST variability within the southwestern Indian Ocean, corresponding to source water for the Agulhas leakage that is thought to play a key role at times of glacial terminations [*Knorr and Lohmann*, 2003; *Peeters et al*., 2004]. If our interpretation of earlier warming for austral winter season temperature during the last deglaciation is correct, an early warming recorded in our Mg/Ca record would imply that early SST shifts at upstream of the Agulhas current correspond to wintertime SST changes. An early warming within the Southern Ocean and its associated sea-ice retreat are thought to be key processes for triggering an abrupt resumption of the Atlantic AMOC at the onset of the Bølling-Allerød [*Knorr and Lohmann*, 2003; *Peeters et al*., 2004]. Transposing our results into such context suggests that the advection of tropical waters during austral winters can play a pivotal role on hydrological processes occurring within the southern ocean. A transient increase in temperature of surface waters advected along the Agulhas current during wintertime may have helped early sea-ice retreat [*Shemesh et al*., 2002] and provided a pathway for exporting excess salt into the South Atlantic (Figure 5f).

## 6. Conclusion

[36] Our results suggest that differences in the timing and SST magnitude of deglacial warming in the tropical Indian Ocean depend on which season is captured by $U^{K'}_{37}$ and Mg/Ca SST signals rather than depositional and/or diagenetic process. The seasonal effect on independent proxy SST records is supported by the transient AOGCMs simulation, in which austral winter and summer SSTs in the Mozambique Channel show a similar phase difference in the timing of warming at of the last deglaciation. The deglacial warming trend attributed to local summer temperatures was likely mediated by changes in the Atlantic Meridional Overturning Circulation at the onset of the deglaciation. In contrast, winter season SSTs were likely mediated by climate changes occurring in the southern hemisphere. The tropical Indian Ocean SSTs history was closely linked to both hemisphere's climate change through annual cycle of Indian monsoon system and its associated heat and moisture transport and storage. Seasonal SST changes can explain the observed proxy-dependent mismatches in deglacial SST timing and help to clarify ongoing debates concerning leads and lags of tropical SSTs with respect to the rises of atmospheric concentrations of greenhouse gases and melting of continental ice sheets. Our study reiterates that multiple SST proxies can go beyond reconstructing the average climate trend and help determining past climate seasonality.

[37] **Acknowledgments.** This project was funded by the German Science Foundation (DFG) and DFG ExCl 80 "the Future Ocean." TL was also supported by JCI-2009-04933. The authors thank the captain, the crew, and the participants of Meteor cruise 75/3. We thank Dr. D. Garbe-Schönberg and staff in the ICP-OES laboratory at CAU for Mg/Ca measurements, S. Koch and C. Rautenstrauch for laboratory assistances, and J. van der Lubbe for fruitful discussion. We are grateful to Drs. Z. Liu, H. Feng, and B. Otto-Bliesner for providing the AOGCMs transient model output for the seasonal sea surface temperature in the Mozambique Channel, and Dr. F. Lombard for discussion about *G. ruber* maximum growth for our sample location. Finally, we thank the associated editor Dr. R. Tada and two anonymous reviewers for their valuable and constructive comments that improved this manuscript.

## References

Anand, P., H. Elderfield, and M. H. Conte (2003), Calibration of Mg/Ca thermometry in planktonic foraminifera from a sediment trap time series, *Paleoceanography*, *18*(2), doi:10.1029/2002PA00846.

Arbuszewski, J., P. deMenocal, A. Kaplan, and E. C. Farmer (2010), On the fidelity of shell-derived δ18O seawater estimates, *Earth Planet. Sci. Lett.*, *300*, 185–196.

Bard, E., F. Rostek, and C. Sonzogni (1997), Interhemispheric synchrony of the last deglaciation inferred from alkenone palaeothermometry, *Nature*, *385*(6618), 707–710.

Bard, E., F. Rosteck, J.-L. Turon, and S. Gendreau (2000), Hydrological impact of Heinrich Events in the subtropical Northeast Atlantic, *Sciences*, *289*, 1321–1324.

Bard, E. (2001), Paleoceanographic implications of the difference in deep-sea sediment mixing between large and fine particles, *Paleoceanography*, *16*(3), 235–239.

Barker, S., M. Greaves, and H. Elderfield (2003), A study of cleaning procedures used for foraminiferal Mg/Ca paleothermometry, *Geochem. Geophys. Geosyst.*, *4*(9), 8407, doi:10.1029/2003GC000559.

Bemis, B. E., H. J. Spero, J. Bijma, and D. W. Lea (1998), Reevaluation of the oxygen isotopic composition of planktonic foraminifera: Experimental results and revised paleotemperature equations, *Paleoceanography*, *13*(2), 150–160.

Bintanja, R., R. S. W. van de Wal, and J. Oerlemans (2005), Modelled atmospheric temperatures and global sea levels over the past million years, *Nature*, *437*(7055), 125–128.

Birch, H., H. K. Coxall, N. P. Paul, D. Kroon, and M. O'Regan (2013), Planktonic foraminifera stable isotope and water column structure: Disentangling ecoloical signals, *Mar. Micropaleontol.*, doi:10.1016/j.marmicro.2013.02.002.

Blanchet, C. L., S. Kasten, L. Vidal, S. W. Poulton, R. Ganeshram, and N. Thouveny (2012), Influence of diagenesis on the stable isotopic composition of biogenic carbonates from the Gulf of Tehuantepec oxygen minimum zone, *Geochem. Geophys. Geosyst.*, *13*, Q04003, doi:10.1029/2011GC003800.

Brown, S. J., and H. Elderfield (1996), Variations in Mg/Ca and Sr/Ca ratios of planktonic foraminifera caused by postdepositional dissolution: Evidence of shallow Mg-dependent dissolution, *Paleoceanography*, *11*(5), 543–551.

Caley, T., et al. (2011), High-latitude obliquity as a dominant forcing in the Agulhas current system, *Clim. Past.*, *7*(4), 1285–1296.

Conkright, M. E., R. A. Locarnini, H. E. Garcia, T. D. O'Brien, T. P. Boyer, C. Stephens, and J. I. Antonov (2002), *World Ocean Atlas 2001: Objective Analyses, Data Statistics, and Figures, CD-ROM Documentation*, 17 pp., National Oceanographic Data Center, Silver Spring, MD.

Conte, M. H., M. A. Sicre, C. Ruhlemann, J. C. Weber, S. Schulte, D. Schulz-Bull, and T. Blanz (2006), Global temperature calibration of the alkenone unsaturation index ($U^{K}_{37}$) in surface waters and comparison with surface sediments, *Geochem. Geophys. Geosyst.*, *7*, Q02005, doi:10.1029/2005GC001054.

de Garidel-Thoron, T., Y. Rosenthal, L. Beaufort, E. Bard, C. Sonzogni, and A. C. Mix (2007), A multiproxy assessment of the western equatorial Pacific hydrography during the last 30 kyr, *Paleoceanography*, *22*, PA3204, doi:10.1029/2006PA001269.

Dekens, P. S., D. W. Lea, D. K. Pak, and H. J. Spero (2002), Core top calibration of Mg/Ca in tropical foraminifera: Refining paleotemperature estimation, *Geochem. Geophys. Geosyst.*, *3*(4), doi:10.1029/2001GC00020.

Delaygue, G., E. Bard, C. Rollion, J. Jouzel, M. Stievenard, J. C. Duplessy, and G. Ganssen (2001), Oxygen isotope/salinity relationship in the northern Indian Ocean, *J. Geophys. Res.*, *106*(C3), 4565–4574.

Denton, G. H., R. F. Anderson, J. R. Toggweiler, R. L. Edwards, J. M. Schaefer, and A. E. Putnam (2010), The Last Glacial Termination, *Science*, *328*(5986), 1652–1656.

de Ruijter, W. P. M., A. Biastoch, S. S. Drijfhout, J. R. E. Lutjeharms, R. P. Matano, T. Pichevin, P. J. van Leeuwen, and W. Weijer (1999),

Indian-Atlantic interocean exchange: Dynamics, estimation and impact, *J. Geophys. Res.*, *104*(C9), 20,885–20,910, doi:10.1029/1998JC900099.
Deschamps, P., N. Durand, E. Bard, B. Hamelin, G. Camoin, A. L. Thomas, G. M. Henderson, J. Okuno, and Y. Yokoyama (2012), Ice-sheet collapse and sea-level rise at the Bølling warming 14,600 years ago, *Nature*, *483*(7391), 559–564.
Du, Y., and S. P. Xie (2008), Role of atmospheric adjustments in the tropical Indian Ocean warming during the 20th century in climate models, *Geophys. Res. Lett.*, *35*, L08712, doi:10.1029/2008GL033631.
Epica-Community-Members (2006), One-to-one coupling of glacial climate variability in Greenland and Antarctica, *Nature*, *444*(7116), 195–198.
Fallet, U., G. J. Brummer, J. Zinke, S. Vogels, and H. Ridderinkhof (2010), Contrasting seasonal fluxes of planktonic foraminifera and impacts on paleothermometry in the Mozambique Channel upstream of the Agulhas Current, *Paleoceanography*, *25*, PA4223, doi:10.1029/2010PA001942.
Fallet, U., J. Ullgren, I. S. Castañeda, H. M. van Aken, S. Schouten, H. Ridderinkhof, and G. J. Brummer (2011), Contrasting variability in foraminiferal and organic paleotemperature proxies in sedimenting particles of the Mozambique Channel (SW Indian Ocean), *Geochim. Cosmochim. Acta*, *75*(20), 5834–5848.
Fallet, U., I. S. Castañeda, A. Henry-Edwards, T. O. Richter, W. Boer, S. Schouten, and G. J. Brummer (2012), Sedimentation and burial of organic and inorganic temperature proxies in the Mozambique Channel, SW Indian Ocean, *Deep Sea Res., Part I*, *59*, 37–53.
Fraile, I., S. Mulitza, and M. Schulz (2009a), Modeling planktonic foraminiferal seasonality: Implications for sea-surface temperature reconstructions, *Mar. Micropaleontol.*, *72*(1–2), 1–9.
Fraile, I., S. Mulitza, M. Schulz, U. Merkel, M. Prange, and A. Paul (2009b), Modeling the seasonal distribution of planktonic foraminifera during the Last Glacial Maximum, *Paleoceanography*, *24*, PA2216, doi:10.1029/2008PA001686.
Friedrich, O., R. Schiebel, P. A. Wilson, S. Weldeab, C. J. Beer, M. J. Cooper, and J. Flebig (2012), Influence of test size, water depth, and ecology on Mg/Ca, Sr/Ca, δ18O and δ13C in nine modern species of planktic foraminifers, *Earth Planet. Sci. Lett.*, *319-320*, 133–145.
Gasse, F., F. Chalie, A. Vincens, M. A. J. Williams, and D. Williamson (2008), Climatic patterns in equatorial and southern Africa from 30,000 to 10,000 years ago reconstructed from terrestrial and near-shore proxy data, *Quat. Sci. Rev.*, *27*(25–26), 2316–2340.
Greaves, M., et al. (2008), Interlaboratory comparison study of calibration standards for foraminiferal Mg/Ca thermometry, *Geochem. Geophys. Geosyst.*, *9*, Q08010, doi:10.1029/2008GC001974.
He, F., J. D. Shakun, P. U. Clark, A. E. Carlon, Z. Y. Liu, B. L. Otto-Bliesner, and J. E. Kutzbach (2013), Northern Hemisphere forcing of Southern Hemisphere climate during the last deglaciation, *nautre*, *494*, 81–85.
Herbert, T. D. (2001), Review of alkenone calibrations (culture, water column, and sediments), *Geochem. Geophys. Geosyst.*, *2*, doi:10.1029/2000GC000055.
Hoogakker, B. A. A., G. P. Klinkhammer, H. Elderfield, E. J. Rohling, and C. Hayward (2009), Mg/Ca paleothermometry in high salinity environments, *Earth Planet. Sci. Lett.*, *284*(3–4), 583–589.
Jaeschke, A., C. Ruhlemann, H. Arz, G. Heil, and G. Lohmann (2007), Coupling of millennial-scale changes in sea surface temperature and precipitation off northeastern Brazil with high-latitude climate shifts during the last glacial period, *Paleoceanography*, *22*, PA4206, doi:10.1029/2006PA001391.
Kiefer, T., and M. Kienast (2005), Patterns of deglacial warming in the Pacific Ocean: A review with emphasis on the time interval of Heinrich event 1, *Quat. Sci. Rev.*, *24*(7–9), 1063–1081.
Kiefer, T., N. McCave, and H. Elderfield (2006), Antarctic control on tropical Indian Ocean sea surface temperature and hydrography, *Geophys. Res. Lett.*, *33*, L24612, doi:10.1029/2006GL027097.
Kienast, M., S. Steinke, K. Stattegger, and S. E. Calvert (2001), Synchronous tropical South China Sea SST change and Greenland warming during deglaciation, *Science*, *291*(5511), 2132–2134.
Kienast, M., S. S. Kienast, S. E. Calvert, T. I. Eglinton, G. Mollenhauer, R. Francois, and A. C. Mix (2006), Eastern Pacific cooling and Atlantic overturning circulation during the last deglaciation, *Nature*, *443*(7113), 846–849.
Knorr, G., and G. Lohmann (2003), Southern Ocean origin for the resumption of Atlantic thermohaline circulation during deglaciation, *Nature*, *424*(6948), 532–536.
Kothawale, D. R., A. A. Munot, and H. P. Borgaonkar (2008), Temperature variability over the Indian Ocean and its relationship with Indian summer monsoon rainfall, *Theor. Appl. Climatol.*, *92*, 31–45.
Koutavas, A., and J. P. Sachs (2008), Northern timing of deglaciation in the eastern equatorial Pacific from alkenone paleothermometry, *Paleoceanography*, *23*, PA4205, doi:10.1029/2008PA001593.
Laepple, T., M. Werner, and G. Lohnmann (2011), Synchronicity of Antarctic temperatures and local solar insolation on orbital timescales, *Nature*, *471*(7336), 91–94.
Lea, D. W., D. K. Pak, and H. J. Spero (2000), Climate impact of late quaternary equatorial Pacific sea surface temperature variations, *Science*, *289*(5485), 1719–1724.
Lea, D. W., D. K. Pak, C. L. Belanger, H. J. Spero, M. A. Hall, and N. J. Shackleton (2006), Paleoclimate history of Galapagos surface waters over the last 135,000 yr, *Quat. Sci. Rev.*, *25*(11–12), 1152–1167.
Leduc, G., R. Schneider, J.- H. Kim, and G. Lohmann (2010), Holocene and Eemian sea surface temperature trends as revealed by alkenone and Mg/Ca paleothermometry, *Quat. Sci. Rev.*, *29*(7–8), 989–1004.
Levi, C., L. Labeyrie, F. Bassinot, F. Guichard, E. Cortijo, C. Waelbroeck, N. Caillon, J. Duprat, T. de Garidel-Thoron, and H. Elderfield (2007), Low-latitude hydrological cycle and rapid climate changes during the last deglaciation, *Geochem. Geophys. Geosyst.*, *8*, Q05N12, doi:10.1029/2006GC001514.
Li, C., D. S. Battisti, D. P. Schrag, and E. Tziperman (2005), Abrupt climate shifts in Greenland due to displacements of the sea ice edge, *Geophys. Res. Lett.*, *32*, L19702, doi:10.1029/2005GL023492.
Linsley, B. K., Y. Rosenthal, and D. W. Oppo (2010), Holocene evolution of the Indonesian throughflow and the western Pacific warm pool, *Nat. Geosci.*, *3*(8), 578–583.
Liu, Z., et al. (2009), Transient Simulation of Last Deglaciation with a New Mechanism for Bølling-Allerød Warming, *Science*, *325*(5938), 310–314.
Lohmann, G., M. Pfeiffer, T. Laepple, G. Leduc, and J.-H. Kim (2012), A model-data comparison of Holocene global sea surface temperature evolution, *Clim. Past Discuss.*, *8*, 100501056.
Lombard, F., L. Labeyrie, E. Michel, E. Bopp, E. Cortijo, S. Ratailleau, H. Howa, and F. Jorissen (2011), Modelling planktic foraminifer growth and distribution using an ecophysiological multi-species approach, *Bigeosciences*, *8*, 853–873.
New, A. L., S. G. Alderson, D. A. Smeed, and K. L. Stansfield (2006), On the circulation of water masses across the Mascarene Plateau in the South Indian Ocean, *Deep Sea Res., Part I*, *54*, 42–74.
MARGO Project Members (2009), Constraints on the magnitude and patterns of ocean cooling at the Last Glacial Maximum, *Nat. Geosci.*, *2*(2), 127–132.
Martrat, B., J. O. Grimalt, N. J. Shackleton, L. de Abreu, M. A. Hutterli, and T. F. Stocker (2007), Four climate cycles of recurring deep and surface water destabilizations on the Iberian Margin, *Science*, *317*, 502–507.
McCorkle, D. C., S. R. Emerson, and P. D. Quay (1985), Stable carbon isotopes in marine porewaters, *Earth Planet. Sci. Lett.*, *74*, 13–26.
McManus, J. F., R. Francois, J. M. Gherardi, L. D. Keigwin, and S. Brown-Leger (2004), Collapse and rapid resumption of Atlantic meridional circulation linked to deglacial climate changes, *Nature*, *428*(6985), 834–837.
Meteor Cruise 75/3 report (2008), *Western Indian Ocean Climate and Sedimentation*, 86 pp., University of Hamburg, Hamburg.
Mix, A. C. (2006), Running hot and cold in the eastern equatorial Pacific, *Quat. Sci. Rev.*, *25*(11–12), 1147–1149.
Mohtadi, M., A. Lückge, S. Steinke, J. Groeneveld, D. Hebbeln, and N. Westphal (2010), Late Pleistocene surface and thermocline conditions of the eastern tropical Indian Ocean, *Quat. Sci. Rev.*, *29*(7–8), 887–896.
Mollenhauer, G., T. I. Eglinton, N. Ohkuchi, R. R. Schneider, P. J. Muller, P. M. Grootes, and J. Rullkotter (2003), Asynchronous alkenone and foraminfera records from the Benguela Upwelling System, *Geochim. Cosmochim. Acta*, *67*(12), 2157–2171.
Mollenhauer, G., M. Kienast, F. Lamy, H. Meggers, R. R. Schneider, J. M. Hayes, and T. I. Eglinton (2005), An evaluation of C-14 age relationships between co-occurring foraminifera, alkenones, and total organic carbon in continental margin sediments, *Paleoceanography*, *20*, PA1016, doi:10.1029/2004PA001103.
Naidu, P. D., and P. Govil (2010), New evidence on the sequence of deglacial warming in the tropical Indian Ocean, *J. Quat. Sci*, *25*(7), 1138–1143.
NGRIP-members (2004), High-resolution record of Northern Hemisphere climate extending into the last interglacial period, *Nature*, *431*(7005), 147–151.
Ohkouchi, N., T. I. Eglinton, L. D. Keigwin, and J. M. Hayes (2002), Spatial and temporal offsets between proxy records in a sediment drift, *Science*, *298*(5596), 1224–1227.
Pailler, D., and E. Bard (2002), High frequency paleoceanographic changes during the past 140000 yr recorded by the organic matter in sediments of the Iberian Margin, *Palaeogeogr. Palaeoclimatol. Palaeoecol.*, *181*(4), 431–452.
Pahnke, K., J. P. Sachs, L. Keigwein, and A. Timmermann (2007), Eastern tropical Pacific hydrologic changes during the past 27,000 years from D/H ratios in alkenones, *Paleoceanography*, *22*, PA4214, doi:10.1029/2007PA001468.

Peeters, F. J. C., R. Acheson, G. J. A. Brummer, W. P. M. de Ruijter, R. R. Schneider, G. M. Ganssen, E. Ufkes, and D. Kroon (2004), Vigorous exchange between the Indian and Atlantic oceans at the end of the past five glacial periods, *Nature*, *430*(7000), 661–665.

Raj, R. P., B. N. Peter, and D. Pushpadas (2010), Oceanic and atmospheric influences on the variability of phytoplankton bloom in the Southwestern Indian Ocean, *J. Mar. Syst.*, *82*(4), 217–229.

Regenberg, M., D. Nürnberg, S. Steph, J. Groeneveld, D. Garbe-Schonberg, R. Tiedemann, and W. C. Dullo (2006), Assessing the effect of dissolution on planktonic foraminiferal Mg/Ca ratios: Evidence from Caribbean core tops, *Geochem. Geophys. Geosyst.*, *7*, Q07P15, doi:10.1029/2005GC001019.

Regenberg, M., D. Nürnberg, J. Schonfel, and G. J. Reichart (2007), Early diagenetic overprint in Caribbean sediment cores and its effect on the geochemical composition of planktonic foraminifera, *Biogeosciences*, *4*(6), 957–973.

Reimer, P. J., et al. (2009), Intcal09 and Marine09 Radiocarbon Age Calibration Curves, 0–50,000 Years Cal Bp, *Radiocarbon*, *51*(4), 1111–1150.

Rincon-Martinez, D., F. Lamy, S. Contreras, G. Leduc, E. Bard, C. Saukel, T. Blanz, A. Mackensen, and R. Tiedermann (2010), More humid interglacials in Ecuador during the past 500 kyr linked to latitudinal shifts of the equatorial front and the Intertropical Convergence Zone in the eastern tropical Pacific, *Paleoceanography*, *25*, PA2210, doi:10.1029/2009PA001868

Rodgers, K. B., G. Lohmann, S. Lorenz, R. Schneider, and G. M. Henderson (2003), A tropical mechanism for Northern Hemisphere deglaciation, *Geochem. Geophys. Geosyst.*, *4*(5), 1046, doi:10.1029/2003GC000508.

Rohling, E. (2007), Progress in paleosalinity: Overview and pressentation of a new approach, *Paleoceanography*, *22*, PA3215, doi:10.1029/2007PA001437.

Rosenthal, Y., T. de Garidel-Thoron, and L. Beaufort (2006), Late Quaternary paleoceanography of the northwestern Pacific: Results from IMAGES program, *Global Planet. Change*, *53*(1–2), 1–4.

Saher, M. H., F. Rostek, S. J. A. Jung, E. Bard, R. R. Schneider, M. Greaves, G. M. Ganssen, H. Elderfield, and D. Kroon (2009), Western Arabian Sea SST during the penultimate interglacial: A comparison of U-37(K′) and Mg/Ca paleothermometry, *Paleoceanography*, *24*, PA2212, doi:10.1029/2007PA001557.

Saraswat, R., D. W. Lea, R. Nigam, A. Mackensen, and D. K. Naik (2013), Deglaciation in the tropical Indian Ocean driven by interplay between the regional monsoon and global teleconnections, *Earth Planet. Sci. Lett.*, *375*, 166–175.

Schneider, B., G. Leduc, and P. Wonsun (2010), Disentangling seasonal signals in Holocene climate trends by satellite-model-proxy integration, *Paleoceanography*, *25*, PA4217, doi:10.1029/2009PA001893.

Shackleton, N. J. (1977), Carbon-13 in Uvigerina: Tropical rainforest history and the equatorial pacific carbonate dissolution cycles in *The Fate of Fossil Fuel CO2 in the Oceans*, edited by N. R. Andersen and A. Malahoff, pp. 401–428, Plenum Publ. Corp, New York.

Shakun, J. D., S. J. Burns, D. Fleitmann, J. Kramers, A. Matter, and A. Al-Subary (2007), A high-resolution, absolute-dated deglacial speleothem record of Indian Ocean climate from Socotra Island, Yemen, *Earth Planet. Sci. Lett.*, *259*(3–4), 442–456.

Shakun, J. D., P. U. Clark, F. He, S. A. Marcott, A. C. Mix, Z. Y. Liu, B. Otto-Bliesner, A. Schmittner, and E. Bard (2012), Global warming preceded by increasing carbon dioxide concentrations during the last deglaciation, *Nature*, *484*(7392), 49–U1506.

Shemesh, A., D. Hodell, X. Crosta, S. Kanfoush, C. Charles, and T. Guilderson (2002), Sequence of events during the last deglaciation in Southern Ocean sediments and Antarctic ice cores, *Paleoceanography*, *17*(4), 1046, doi:10.1029/2000PA000599.

Sicre, M. A., L. Labeyrie, U. Ezat, J. Duprat, J. L. Tron, S. Schmidt, E. Michel, and A. Mazaud (2005), Mid-latitude Southern Indian Ocean response to Northern Hemisphere Heinrich events, *Earth Planet. Sci. Lett.*, *240*(3–4), 724–731.

Siddorn, J. R., D. G. Bowers, and A. M. Hoguane (2001), Detecting the Zambezi River plume using observed optical properties, *Mar. Pollut. Bull.*, *42*(10), 942–950.

Sonzogni, C., E. Bard, F. Rostek, D. Dollfus, A. Rosell-Mele, and G. Eglinton (1997), Temperature and salinity effects on alkenone ratios measured in surface sediments from the Indian Ocean, *Quat. Res.*, *47*(3), 344–355.

Stanford, J. D., E. J. Rohling, S. Bacon, A. P. Roberts, F. E. Grousset, and M. Bolshaw (2011), A new concept for the paleoceanographic evolution of Heinrich event 1 in the North Atlantic, *Quat. Sci. Rev.*, *30*, 1047–1066.

Steinke, S., M. Kienast, J. Groeneveld, L. C. Lin, M. T. Chen, and R. Rendle-Buhring (2008), Proxy dependence of the temporal pattern of deglacial warming in the tropical South China Sea: Toward resolving seasonality, *Quat. Sci. Rev.*, *27*(7–8), 688–700.

Stuiver, M., and P. J. Reimer (1993), Extended C-14 data-base and revised calib 3.0 C-14 age calibration program, *Radiocarbon*, *35*(1), 215–230.

Trauth, M. H., M. Sarnthein, and M. Arnold (1997), Bioturbational mixing depth and carbon flux at the seafloor, *Paleoceanography*, *12*(3), 517–526, doi:10.1029/97PA00722.

van der Lubbe, J., R. Tjallingii, G. J. Brummer, and R. R. Schneider (2012), Terrigenous sediment transport and deposition along the Mozambique margin during the last deglacial period, paper presented at AGU Champman, Stellenbosch, Western Cape, South Africa.

Visser, K., R. Thunell, and L. Stott (2003), Magnitude and timing of temperature change in the Indo-Pacific warm pool during deglaciation, *Nature*, *421*(6919), 152–155.

Wang, Y. V., T. Larsen, G. Leduc, N. Andersen, T. Blanz, and R. R. Schneider (2013), What does leaf wax δD from a mixed C3/C4 vegetation region tell us?, *Geochim. Cosmochim. Acta*, *111*, 128–139.

Weldeab, S., R. R. Schneider, and M. Kölling (2006), Deglacial sea surface temperature and salinity increase in the western tropical Atlantic in synchrony with high latitude climate instabilities, *Earth Planet. Sci. Lett.*, *241*(3–4), 699–706.